A Wide Input Power Line Energy Harvesting Circuit for Wireless Sensor Nodes

Jinhua Wang

Thesis submitted to the faculty of the Virginia Polytechnic Institute and State University
in partial fulfillment of the requirements for the degree of

Master of Science
In
Electrical Engineering

Dong S. Ha, Chair
Yang Yi
Xiaoting Jia

Apr. 28th, 2021
Blacksburg, Virginia

Keywords: powerline energy harvesting, current transformer, buck-boost convertor, impedance matching, maximum power point (MPP), wireless sensor network (WSN)

A Wide Input Power Line Energy Harvesting Circuit for Wireless Sensor Nodes

Jinhua Wang

ABSTRACT

Massive deployment of wireless IoT (Internet of Things) devices makes replacement or recharge of batteries expensive and impractical for some applications. Energy harvesting is a promising solution, and various designs are proposed to harvest power from ambient resources including thermal, vibrational, solar, wind, and RF sources. Among these ambient resources, AC powerlines are a stable energy source in an urban environment. Many researchers investigated methods to exploit this stable source of energy to power wireless IoT devices.

The proposed circuit aims to harvest energy from AC powerlines with a wide input range of from 10 to 50 A. The proposed system includes a wake-up circuit and is capable of cold-start. A buck-boost converter operating in DCM is adopted for impedance matching, where the impedance is rather independent of the operation conditions. So, the proposed system can be applicable to various types of wireless sensor nodes with different internal impedances. Experimental results show that the proposed system achieves an efficiency of 80.99% under the powerline current of 50 A.

A Wide Input Power Line Energy Harvesting Circuit for Wireless Sensor Nodes

Jinhua Wang

GENERAL AUDIENCE ABSTRACT

Nowadays, with the magnificent growth of IoT devices, a reliable, and efficient energy supply system becomes more and more important, because, for some applications, battery replacement is very expensive and sometimes even impossible. At this time, a well-designed self-contained energy harvesting system is a good solution. The energy harvesting system can extend the service life of the IoT devices and reduce the frequency of charging or checking the device.

In this work, the proposed circuit aims to harvest energy from the AC power lines, and the harvested power intends to power wireless sensor nodes (WSNs). By utilizing the efficient and self-contained EH system, WSNs can be used to monitor the temperature, pressure, noise level and humidity etc.

The proposed energy harvesting circuit was implemented with discrete components on a printed circuit board (PCB). Under a power line current of 50 A @ 50 Hz, the proposed energy harvesting circuit can harvest 156.6 mW, with a peak efficiency of 80.99 %.

.

Acknowledgements

My sincerest thanks to my advisor Dr. Dong Sam Ha, for his knowledge, motivation, leadership, and generous guidance throughout my graduate study. There would be no way for me to accomplish this work without his advising. Besides the academic work, we also enjoyed life together, which would be a fantastic memory in my life. I would like to also thank my committee member, Dr. Xiaoting Jia too, for her kind recommendation and help for me to enter graduate school. I would like to also thank my committee member Dr. Yang Yi, for her help when I had encountered difficulties in my studies.

I would like to thank my peers in the MICS group: Ryan Reed, Fabiha Nowshin, Fairborz Lohrabi Pour, Rajesh Kudupudi, Kang Jun Bai, Jiayu Li, Junjie Wang, Yibin Liang, Hongyu An, Abhishek Damle, Xingye Liu, Shiya Liu, Jiayuan Zhang, Moqi Zhang, Victor Gan, Keyvan Ramezanpour. Thank you all for your great help in answering my questions and providing such a great work environment. I hope you all succeed in the future.

Finally, I would like to thank my father, Li Wang, my mother, Hua Xi. I stood on their shoulders and saw the scenery in this world that they had never seen in their lives. Without them, I could not accomplish anything. I would like to also thank my girlfriend, Qing Zhou, for her love and patience over these years. She has always supported me when I encountered any difficulties.

Thank you all, from the bottom of my heart.

Table of Contents

List of Figures

List of Abbreviations

AC	Alternating Current
B-H	Magnetic Flux Density – Magnetic Field Strength
DC	Direct Current
DCM	Discontinuous Conduction Mode
EH	Energy Harvesting
IoT	Internet of Things
MFEH	Magnetic Field Energy Harvester
MPPT	Maximum Power Point Tracking
NVC	Negative Voltage Converter
PMC	Power Management Circuit
RF	Radio Frequency
WSNs	Wireless Sensor Nodes

Chapter 1: Introduction

1.1 Background of Power Line Energy Harvesting System

Massive deployment of wireless IoT (Internet of Things) devices makes replacement or recharge of batteries expensive and impractical for some applications. Energy harvesting is a promising solution, and various designs are proposed to harvest power from ambient resources including thermal, vibrational, solar, wind, and RF sources [1]-[5]. Among these ambient resources, AC powerlines are a stable energy source in an urban environment. Many researchers investigated methods to exploit this stable source of energy to power wireless IoT devices [6]-[10].

The latest and off-the-shelf energy harvesting (EH) technologies, such as vibration energy harvesting products and indoor or wearable photovoltaic cells, generate mW power under typical working conditions. Although the power of this magnitude may seem limited, the continuous operation of energy harvesting components such as wireless sensor nodes (WSNs) for several years may mean that energy harvesting products and long-life batteries are roughly equivalent. Although the battery claims to be able to provide up to 10 years of life, this depends greatly on the level of power taken from it and how often it is drawn. A system with energy harvesting capability can generally be recharged after the power is completely exhausted, but a system powered by only a battery cannot do this, and the disposal of the used batteries is also a serious environmental problem now.

In order to improve the reliability of the EH system, many implementations use some kind of environmental energy source as the main power source and use the battery as a supplement to the environmental energy source. If the environmental energy source disappears or is interrupted, the main battery can be connected to power the load. This can be thought of as a "battery life extender" capability that can provide the system with longer working life, which is usually about 12 years.

Major design challenges of magnetic field energy harvesters for powerline energy harvesting include saturation and nonlinearity of the core, the geometry of the core, and positioning of the harvester, and distance of harvesting devices from the AC power lines [11]-[16]. The power factor is another issue due to the inductive nature of magnetic field energy harvesters [17]. The core saturation and nonlinearity are investigated, and an efficient energy harvester is presented in [18]. Design issues for power management circuits for power line energy harvesting include such as impedance matching, underline current and load variations, wake-up circuit, cold-start, and output voltage regulation [12]-[18]. Impedance matching is often achieved by adjusting the duty cycle and the switching frequency of the DC-DC converter [20]-[23], [19], [22] and maximum power point tracking (MPPT) schemes aim to maintain impedance matching under varying operating conditions [4], [24] and [25].

1.2 Proposed Work and Technical Contribution

This thesis proposes a power management circuit (PMC) for collecting energy from railway power lines to power wireless sensor nodes (WSNs).We designed a magnetic field energy harvesting system for railroad power lines, whose current changes a wide range from 10 A to 50 A. Accordingly, the power stage is designed to withstand a wide range of the input current. A buck-boost converter working in discontinuous conduction mode (DCM) is adopted for impedance matching, as the input impedance is ideally independent of the operating conditions such as input, output voltages and load resistance.

1.3 Organization of this Thesis

This thesis is organized as follows. Chapter 2 reviews necessary preliminaries including current transformer characteristics and modeling circuit, DC-DC converter design, impedance matching and existing power line energy harvesting circuits. Chapter 3 discusses the proposed circuit and describes the operation of individual blocks. Chapter 4 presents an experiment setup and measurement results. Chapter 5 concludes the thesis, propose the possible improvements for future work.

Chapter 2: Preliminaries

2.1 Current Transformer Characteristics and Modeling Circuit

Current transformer is an instrument that converts a large current on the primary side into a small current on the secondary side based on the concept of electromagnetic induction. The current transformer is commonly used in high current measurement and non-contact measurement. The current transformer is composed of a closed core and windings. It has a few primary turns (e.g., 1, 2 and 5 turns) and is placed in series with the current path that needs to be measured. The number of turns on the secondary side is relatively large.

When the current transformer is working, its secondary circuit is always closed, and it can be short-circuited. The current transformer converts the large current in the primary side into a small current on the secondary side for measurement, and the secondary side cannot be opened.

Because of the electromagnetic induction of the current transformer, we used it as a magnetic field energy harvester (MFEH) in the proposed energy harvesting system. This section introduces its working principle, parameter description, usage introduction, etc.

2.1.1 Current Transformer Characteristics

A magnetic field energy harvester (MFEH) shown in Figure 2.1 is composed of a winding coil around a ferrite core. It is in essence a current transformer and is used as an energy harvesting device for powerlines [8], [9], [11], [17]. The number of turns of the coil and the ferrite core geometry determines the potential of the device to harvest electromagnetic power as investigated in [9]. An equivalent circuit model considering nonlinearities is presented in [26], and an efficient magnetic field energy harvester is presented in [14].

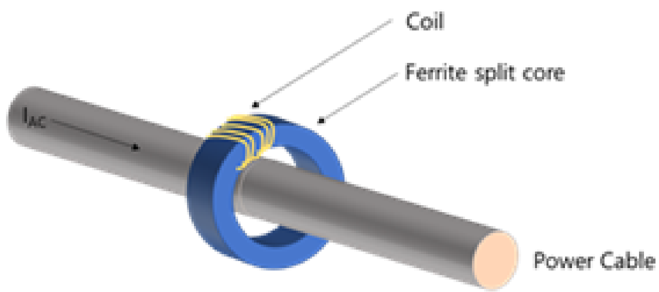

Figure 2.1 Magnetic field energy harvester.

The current transformer is nothing but just a normal voltage transformer with a very small number of turns of the primary side. It means that the primary-secondary equations (1) and (2) for voltage transformer still apply to the current transformer.

$$I_S = I_P \cdot \frac{N_P}{N_S} \tag{1}$$

$$V_S = V_P \cdot \frac{N_S}{N_P} \tag{2}$$

In the proposed power line energy harvesting circuit, the number of turns of the primary side is 1. So (1) and (2) become (3) and (4).

$$I_S = \frac{I_P}{N_S} \tag{3}$$

$$V_S = V_P \cdot N_S \tag{4}$$

Note that for voltage transformer, the secondary side cannot by short-circuited, and for current transformer, the secondary side cannot be open-circuited. If the secondary side of a current transformer is open-circuited, from a perspective of personnel protection, it will be dangerous because of the super high voltage from the secondary side terminals. Assume the primary side is connected to an AC power supply of 220 V at 50 Hz, and $N_P : N_S$ = 1 : 500. From (4), we can get,

$$V_S = V_P \cdot N_S = 220 \cdot 500 = 110\ kV \tag{5}$$

which can cause a deadly electric shock to human beings.

And from a perspective of device protection, the magnetic core will be deeply saturated, and it can be overheated and damaged permanently. According to the Lenz's law, "an induced current flows in a direction such that the current opposes the change that induced it". Figure 2.2 shows the directions of the primary and secondary side currents in difference winding cases.

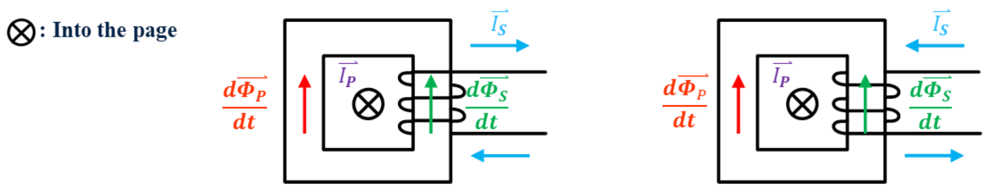

Figure 2.2 Secondary side currents in different cases.

When the secondary side of the current transformer is open-circuited, because the secondary side current is almost 0, the secondary side cannot generate the opposite magnetic flux change $\frac{d\overrightarrow{\Phi_S}}{dt}$ to oppose the primary side magnetic flux change $\frac{d\overrightarrow{\Phi_P}}{dt}$, which means,

$$\frac{d\overrightarrow{\Phi_P}}{dt} \gg \frac{d\overrightarrow{\Phi_S}}{dt}, \tag{6}$$

The magnetic core of the current transformer is instantaneously saturated, and a large eddy current is induced inside the core. A large amount of power is consumed by the core, and it is known as the core loss, which is the major loss for transformers, and the core could be damaged permanently.

2.1.2 Magnetic Core Material Characteristics

Figure 2.3 shows a general B-H curve for the magnetic core materials. The magnetization characteristics of strong magnetic materials under an alternating magnetic field are more complicated due to the existence of hysteresis, eddy current, skin effect, and magnetic aftereffect. These characteristics not only depend on the magnetic properties of the material, but also related to the thickness (sheet) and diameter (linear) of the material, the frequency of the alternating magnetic field, the conductivity, and the excitation waveform. In this way, there are a variety of AC magnetization curves. But the "magnetization curve" measured at this time is no longer the intrinsic B-H curve of the material, but only a certain equivalent magnetization characteristic obtained under specific conditions. The AC magnetization characteristics of each material are only suitable for the occasions where the material is consistent with its test conditions.

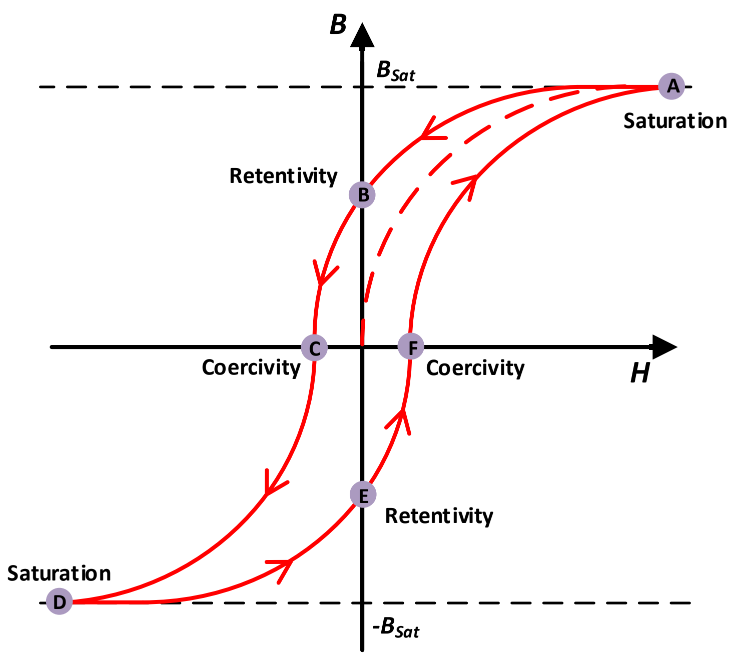

Figure 2.3 B-H curve of magnetic core material.

To simplify the analysis of the B-H characteristics of MFEH, [27] derives a linearized expression for the B-H relationships. Figure 2.4 shows the idealized B-H curve.

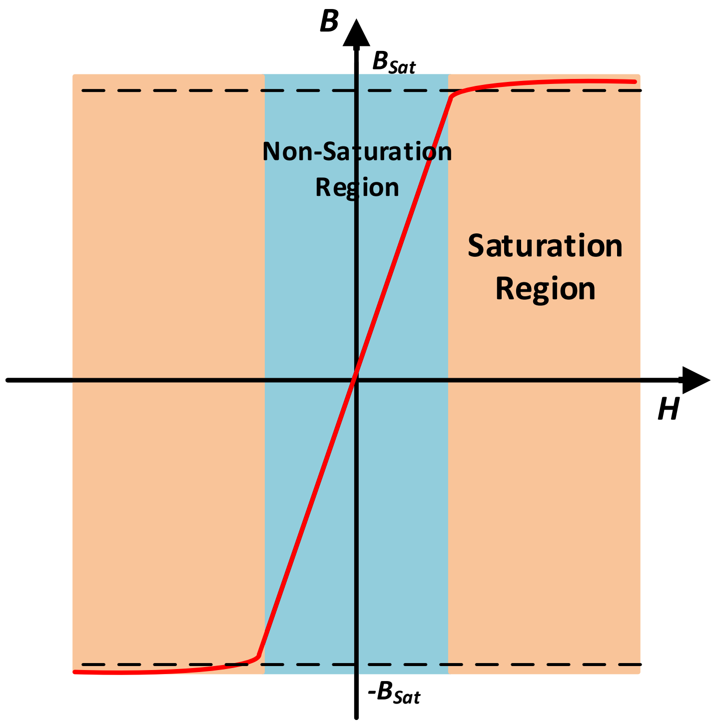

Figure 2.4 Idealized B-H curve.

In order to harvest energy from AC power lines, the MFEH needs to operate in non-saturation region, which is represented in red in Figure 2.4. If the MFEH operates in saturation region, as the magnetic field strength *H* changes , the magnetic field flux density B nearly does not change, result in a very small magnetic flux change ($\frac{d\vec{\Phi}}{dt}$). So, there is almost no induced current in the secondary side. Meanwhile, a large eddy current will be induced inside the magnetic core, and a large amount of energy will be dissipated by the magnetic core. Under this condition for a long time, the magnetic core can be overheated, and possibly damaged permanently.

2.1.3 Modeling Circuit

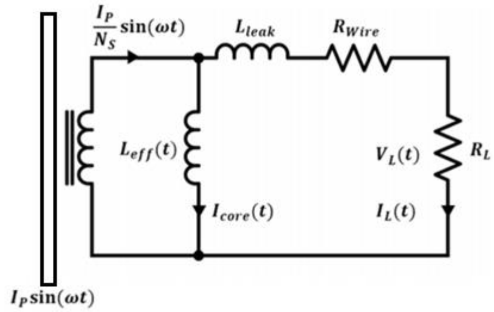

Figure 2.5 Equivalent circuit of current transformer.

Figure 2.5 shows an equivalent circuit of current transformer used in the proposed circuit. Because the number of turns of the primary is 1, the primary side is represented by a wire. When the current in the primary side is $I_P Sin(\omega t)$, according to (3), the current in the secondary side is $\frac{I_P}{N_S} Sin(\omega t)$. $L_{eff}(t)$ is the effective inductance of the current transformer, and it is a function of the time, or more clearly speaking, it is a function of the magnetic field strength.

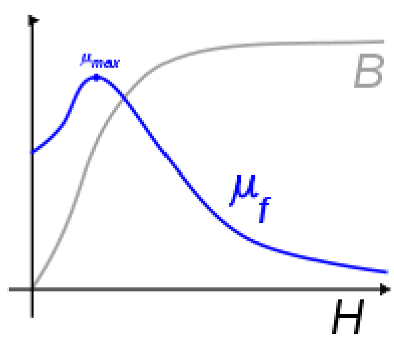

Figure 2.6 B-μ-H curve of a magnetic core material.

As shown in Figure 2.6, as magnetic field strength H increases, firstly, the permeability of the core material increases, and it reaches a peak value. Then, it starts to decrease, until it reaches approximately 0. The secondary side effective inductance is defined in (7),

$$L_{eff} = \frac{N_S^2 \mu A}{L} \tag{7}$$

So, the secondary side effective inductance is not a constant, but a function of the permeability μ of the material.

L_{leak} is the leakage inductance of the current transformer, and it is modeled in series with the effective inductance as shown in Figure 2.7. R_{wire} is the wire resistance. In analysis of the proposed power line EH circuit, because L_{leak} and R_{wire} are very small, they are ignored.

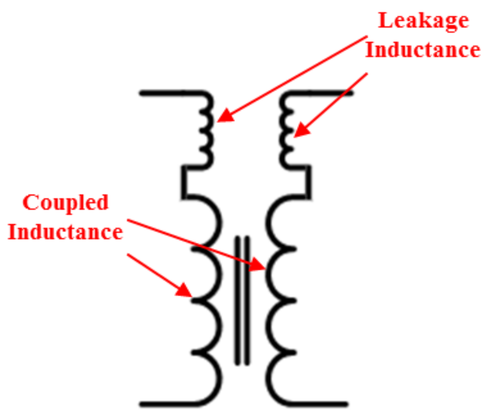

Figure 2.7 Inductance modeling of current transformer.

2.1.4 Operation of the Current Transformer

Just like all kinds of transformers, current transformer only works under an AC power supply. The operation of the current transformer is well-defined through (8) – (11).

$$\vec{H} = \int_{R1}^{R2} \frac{\overrightarrow{I_P}}{2\pi r} dr \tag{8}$$

$$\vec{B} = \mu \vec{H} \tag{9}$$

$$\vec{\Phi} = \vec{B} S \tag{10}$$

$$\overrightarrow{I_S} \propto \frac{d\vec{\Phi}}{dt} \tag{11}$$

When the primary side of the current transformer is connected to an AC power supply, the primary side generates a magnetic field, whose strength is defined in (8). Accordingly, magnetic flux is generated, and its density and magnitude are defined in (9) and (10), respectively. Because the amplitude of the primary side current changes as time changes, a magnetic flux change is generated, and because of it, an AC current is induced in the secondary side, which is defined in (11).

2.2 Negative Voltage Converter (NVC)

Rectification is required for the AC current induced in the secondary side of the current transformer, which can be done by using a full-bridge rectifier. However, for small-scale energy harvesting systems, the system itself should dissipate as less power as possibly, but even consisting of Schottky diodes, a full-bridge rectifier consumes a relatively large amount of power. Figure 2.8 shows negative voltage converter (NVC) that performs rectification with a reduced power consumption [28]-[30]. The idea is firstly introduced in IC design, because in IC design, Schottky diode cannot be implemented on-chip. Because the input terminals of the NVC is connected to an AC source, if the input voltage is in the positive half cycle, the MOSFETs M_1 and M_4 are conducting and the current flow starts from the positive terminal, which is denoted as node A through M_1 and D_1 to the load, and goes back to the negative terminal, which is denoted as node B through MOSFET M_4. The current path is the opposite during the negative half cycle. Diode D_1 prevents backflow of current from the load when the load voltage (possible in transients) is higher than the source voltage. The voltage drop from the drain to the source of the turned-on transistor is small, so the NVC consumes less power. Note that the direction of the body diode of the transistor matches the direction of the current.

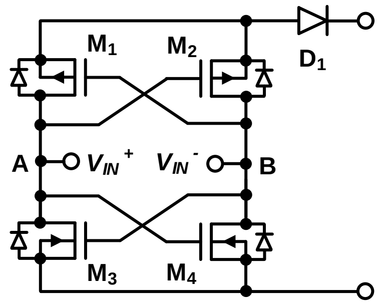

Figure 2.8 Negative voltage converter (NVC).

2.3 DC-DC Converters and Impedance Matching

Usually, in power electronics applications, DC-DC converters are used to effectively output a fixed voltage after converting the input voltage. DC-DC converters are categorized into three basic topologies: buck converter, boost converter, and buck-boost converter. Three topologies can be used according to the application requirements. Usually, these converters are controlled by PWM, and they have high efficiency and good output voltage ripple and noise. DC-DC converters are widely used in electronics such as mobile phones, chargers, digital cameras, etc. However, in the proposed power line energy harvesting circuit, the DC-DC converter is not used for outputting a fixed voltage, but for impedance matching due to the characteristics of the input resistance of DC-DC converters. In this section, there basic topologies of DC-DC converters and their input resistance characteristics are introduced.

2.3.1 Buck-boost Converter

Figure 2.9 shows an inverting buck-boost converter is shown. Different from the polarity configuration of non-inverting buck-boost converter, which is controlled by four switches, for an inverting buck-boost converter, the polarities of the output voltage are opposite to the input voltage. The input resistance of a buck-boost converter operating in DCM is given in (12) [22],

$$R_{in} = \frac{2\mathrm{L}}{\mathrm{D}_1^2 T_s} \tag{12}$$

where L is the inductance, D_1 is the duty cycle, and T_S is the switching period of the converter. As (11) shows, ideally, the input resistance of an inverting buck-boost converter operating in DCM is independent of the operating conditions, such as input voltage, output voltage and load resistance. But in the real world, the input resistance of buck-boost converter operating in DCM is not completely independent of the operating conditions, which will be further investigated in Chapter 4. And buck-boost converter usually performs the lowest efficiency among buck, boost, and buck-boost converters [23].

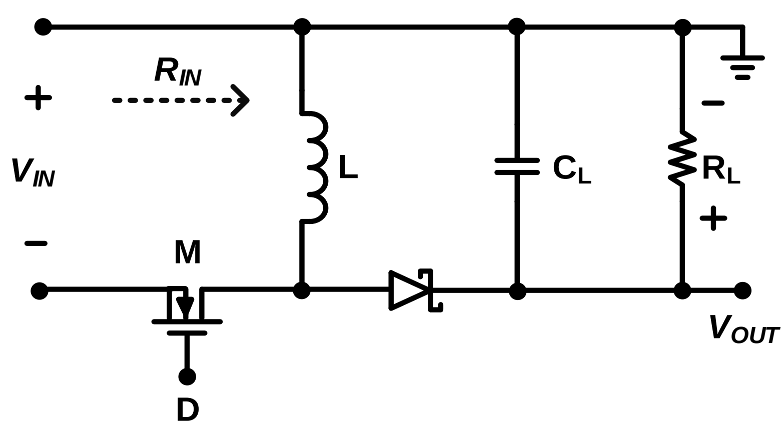

Figure 2.9 Inverting buck-boost converter topology.

2.3.2 Buck Converter

Figure 2.10 shows a circuit diagram of buck converter, and its input resistance in DCM is given in (13) [31],

$$R_{in} = \frac{2L}{\left(1 - \frac{V_{OUT}}{V_{IN}}\right) D_1^2 T_S} \tag{13}$$

And,

$$\frac{V_{OUT}}{V_{IN}} = \frac{2}{\sqrt{1 + \frac{8L}{\sqrt{D_1^2 R_L T_S}}}} \tag{14}$$

where all the parameters are as same as those of buck-boost converter, except for R_L, which is the load resistance. Compared to buck-boost converter, the input impedance of buck converter is dependent on the load resistance, which theoretically reduces the reliability of the circuit.

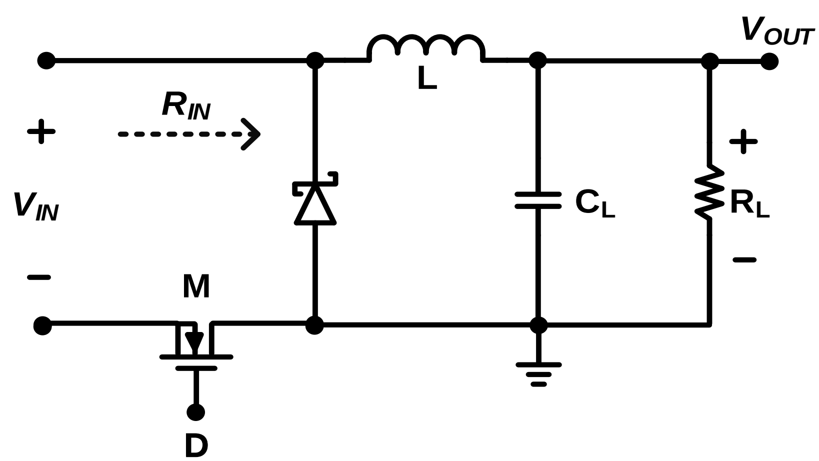

Figure 2.10 Buck converter topology.

2.3.3 Boost Converter

A Boost converter is shown in Figure 2.11, and its input resistance in DCM is given in (15) [31],

$$R_{in} = \frac{2\mathrm{L}}{D_1^2 T_S}\left(1 - \frac{V_{IN}}{V_{OUT}}\right) \tag{15}$$

And,

$$\frac{V_{IN}}{V_{OUT}} = \frac{2}{1 + \sqrt{1 + \frac{4D_1^2 R_L T_S}{2L}}} \tag{16}$$

where all the parameters are as same as those of the buck converter.

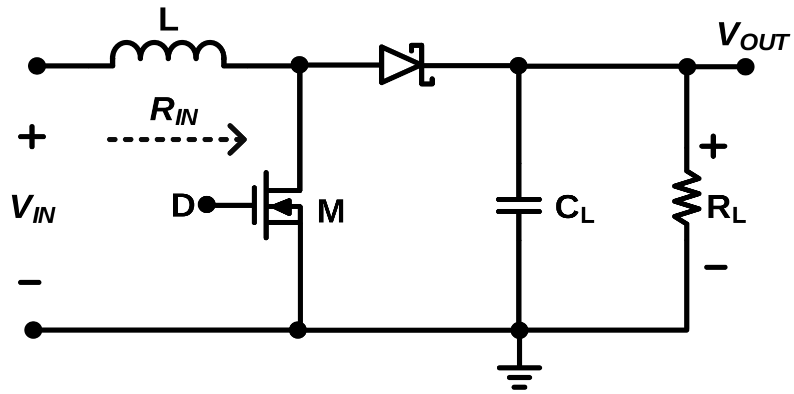

Figure 2.11 Boost converter topology.

2.4 Previous Works

Zhuang et al. proposed a circuit, in which the core of the MFEG is ensured not in the saturation mode [8]. Noting that instantaneous power can be much larger for a short time period than the average power for a long time period, the circuit aims to power the load for a short period with large energy. After charging the storage capacitor for 190 ms from a powerline current of 10 A, the circuit extracts 792 mW from the power line. In order to avoid saturation of the core of the MFEG, a switch is added to the circuit to short the circuit of the core, when the coil reaches saturation.

Taithongchai and Leelarasmee presented a circuit design to harvest 58 mW from a powerline with 65 A of line current [10]. A boost converter dynamically adjusts the input impedance to implement MPPT, which is based on the feedback of the output voltage. A low-power microcontroller PIC16F690 is used to adjust the duty cycle of the boost converter. One shortcoming of the design is the inability to regulate the output voltage, and so that the circuit may be used to recharge batteries but not to power sensor nodes directly. Also, the circuit is limited to harvest energy only from large powerline current ranging from 65 A to 130 A

Zeng et al. presented an MFEH for 3-Phase 10 kV powerlines [32]. The system uses an off-the-shelf MAX17710 energy harvesting IC, which limits the maximum input voltage to 6 V, therefore resulting in a limit of the harvested power of the system.

Chapter 3: Proposed Power Line EH Circuit

3.1 Block Diagram

Figure 3.1 shows the block diagram of the proposed circuit for powerline energy harvesting. As an MFEH starts to harvest power from a powerline, the rectifier charges the wake-up circuit to activate the oscillator (OSC), which in turn activates the buck-boost converter. A buck-boost converter provides impedance matching to extract the maximum power. The voltage regulator regulates the output voltage to 3.3 V to power the load, i.e., sensors.

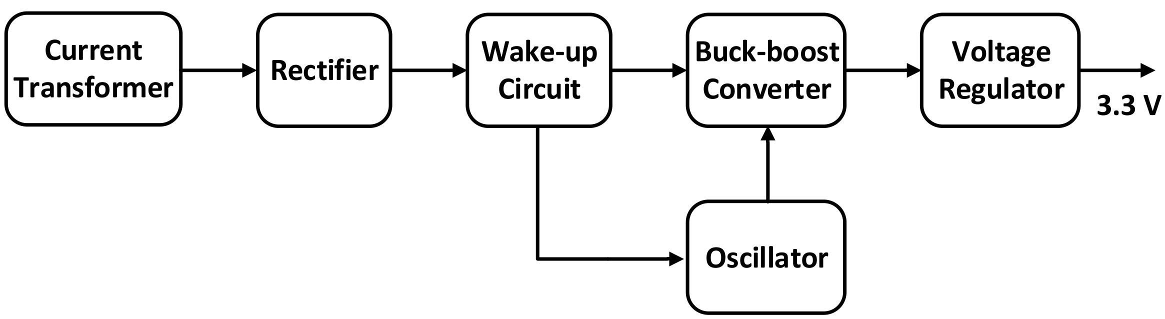

Figure 3.1 System block diagram.

3.2 Wake-up Circuit

When the MFEH starts to generate power from a powerline, it charges capacitor C_1 through R_1 of the wake-up circuit in Fig. 4. The capacitor voltage V_{OSC} provides power to the oscillator. When the voltage reaches 3 V, the oscillator starts to oscillate, which activates the buck-boost converter. When the MFEH does not generate power, the V_{OSC} approaches to 0. Hence, the oscillator becomes inactive to save the power dissipation of the converter. The breakdown voltage of the diode D_1 is 5 V, which regulates the maximum capacitor voltage V_{OSC}.

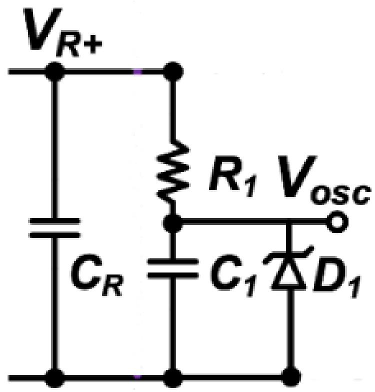

Figure 3.2 Wake-up circuit.

3.3 Oscillator

Figure 3.3 shows the oscillator. It generates pulse waves with a fixed frequency and duty cycle. It is adopted in the proposed design [22]. The switching frequency and the duty cycle of the oscillator can be approximately expressed as (17) and (18), respectively, if $R_2 >> R_1$. The switching frequency and duty cycle can be tuned by adjusting the values of R_1, R_2 and C_1, and in practice, R_1 and R_2 can be variable resistors. The output voltage V_{GATE} drives the gate of a buck-boost converter for the proposed design.

$$f \approx \frac{1}{(R_1 + R_2)C_1 ln2} \tag{17}$$

$$D \approx \frac{R_1}{R_2} \tag{18}$$

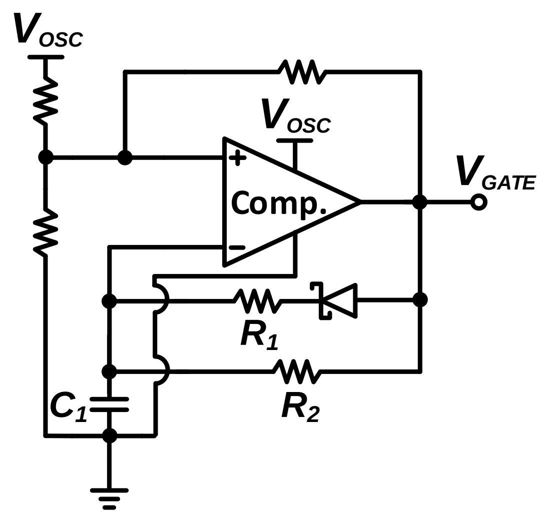

Figure 3.3 Oscillator.

3.4 Buck-boost Converter for Impedance Matching

An inverting buck-boost converter is adopted for impedance matching in the proposed circuit. The input resistance of the buck-boost converter is set to 2 kΩ. The driving pulses signals are generated by an oscillator.

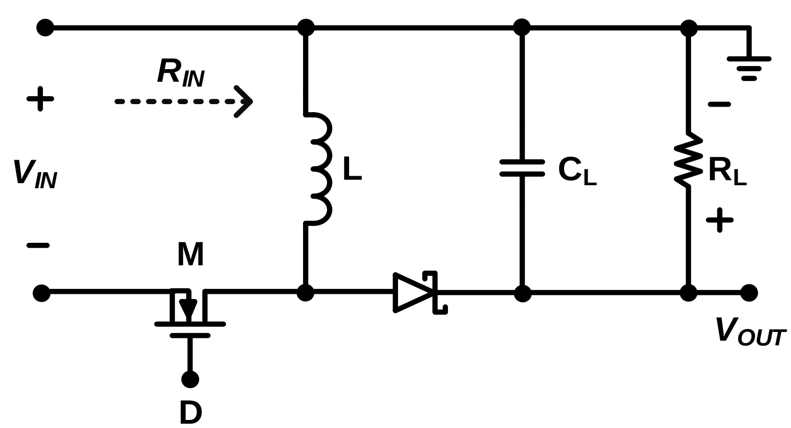

Figure 3.4 Buck-boost converter for impedance matching.

3.5 Operation of the Proposed Circuit

A complete circuit diagram of the proposed PMC is shown in Figure 3.5. The MFEH, noted as the current transformer, generates an AC voltage harvested from the powerline current. The NVC is implemented with Schottky diodes for high efficiency. The inductor L_1 of the converter is 15 mH and the capacitor C_O is 100 μF. Based on simulation results, the input impedance of the buck-boost converter is set to 2 kΩ to match the source impedance of the current transformer followed by the rectifier and the wake-up circuit. The voltage regulator provides regulated 3.3 V DC for the load such as sensors, and it is an off-the-shelf IC Analog LT8608.

The proposed system is capable of cold start. Assume that the wake-up circuit capacitor C_1 is completely exhausted, and all other blocks in Figure 3.5 are deactivated. As the MFEH generates induced voltage out of the powerline, the full-bridge rectifier composed of passive diodes charges the capacitor C_1. When the capacitor voltage V_{OSC} reaches 3 V, it activates the oscillator and then the buck-boost converter.

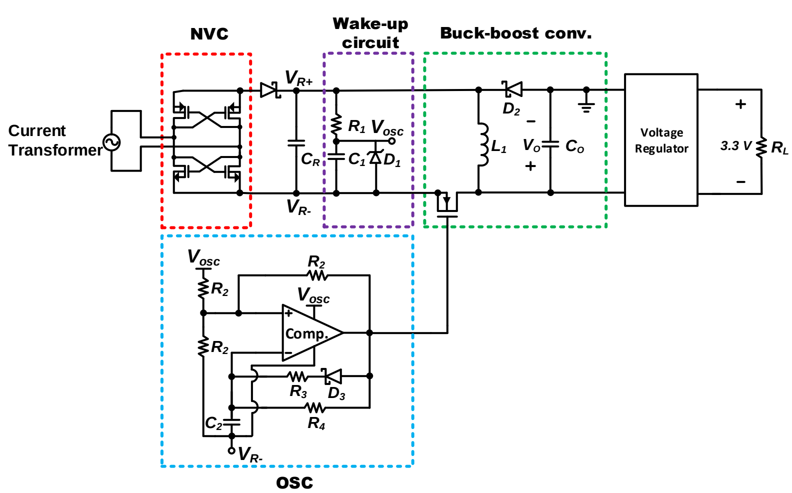

Figure 3.5 Proposed power management circuit.

Chapter 4: Simulation Results

Before being sent to PCB fabrication, the circuit is simulated in LTSpice to verify the functionalities. In this chapter, the simulation results for each block are presented, and simulation results for the complete system are shown at the end.

4.1 MFEH Modeling

For the proposed energy harvesting system, our group focus on the power management circuit part, and the MFEH was designed by other teams. So in our simulation, the MFEH is simply modeled as a voltage source in series with a resistor. And we measured the internal resistance of the MFEH is about 2 kΩ. Based on the concept of impedance matching, the maximum output power is achieved when the load impedance is matched to the source impedance. As the source impedance is modeled purely resistive, the load should be purely resistive too. For the voltage source, the voltage is set to 20 V_{Peak} at a frequency of 60 Hz. Figure 4.1 shows the schematic of the MFEH modeling circuit with an optimal load resistance of 2 kΩ.

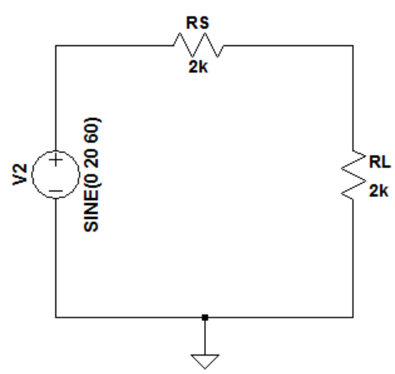

Figure 4.1 MFEH modeling circuit with optimal load resistance.

Figure 4.2 shows the waveforms of the maximum output power of MFEH. As the source generates AC voltage, the output voltage should be represented in RMS value, and the maximum output power is calculated as follows.

$$P_{Max} = \frac{V_{RMS,Out}^2}{R_L} \tag{19}$$

The simulation results prove the calculation. Under an optimal load resistance, the output voltage is 7.04 V, and the output power is 24.61 mW. The maximum power is used as a reference power to calculate the efficiency of the system.

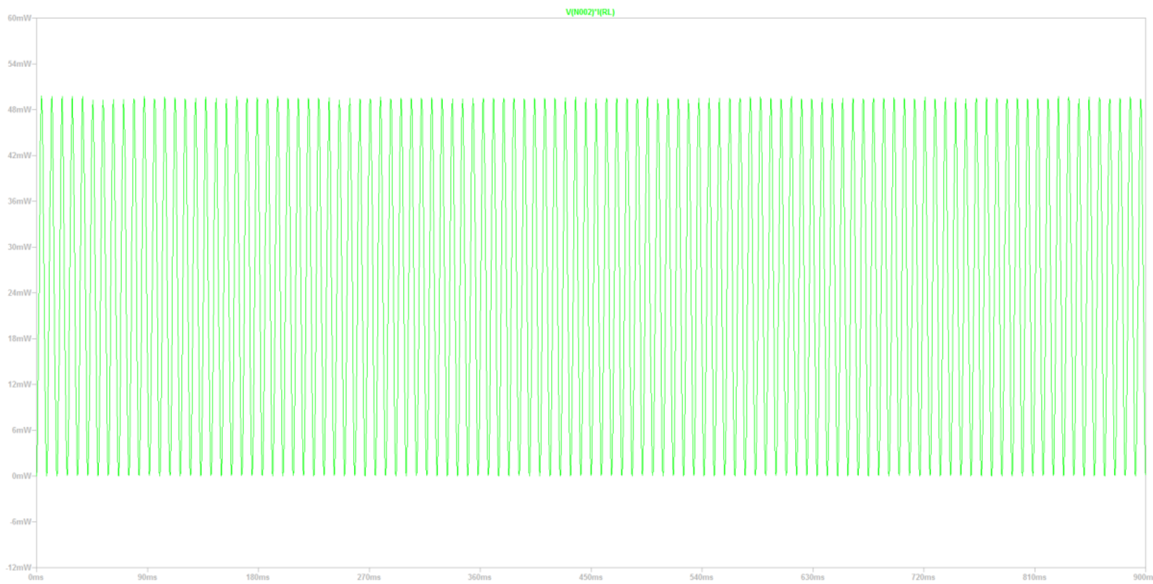

Figure 4.2 Maximum output power of MFEH.

4.2 Negative Voltage Converter (NVC)

As introduced in Chapter 2, a NVC is adopted to rectify the induced AC voltage from the power lines. M_1 and M_2 are PMOS RSS070P05 and M_3 and M_4 are NMOS RSS070N05. The absolute value of the rating voltage for the MOSFETs is 45 V, and the turn-on resistance is 19 mΩ. The Schottky diode PMEG4005AEA is used in simulation. It has a breakdown voltage of 40 V and maximum forward current of 0.5 A. Figure 4.3

shows the LTSpice schematic of the proposed NVC connected to the MFEH modeling circuit.

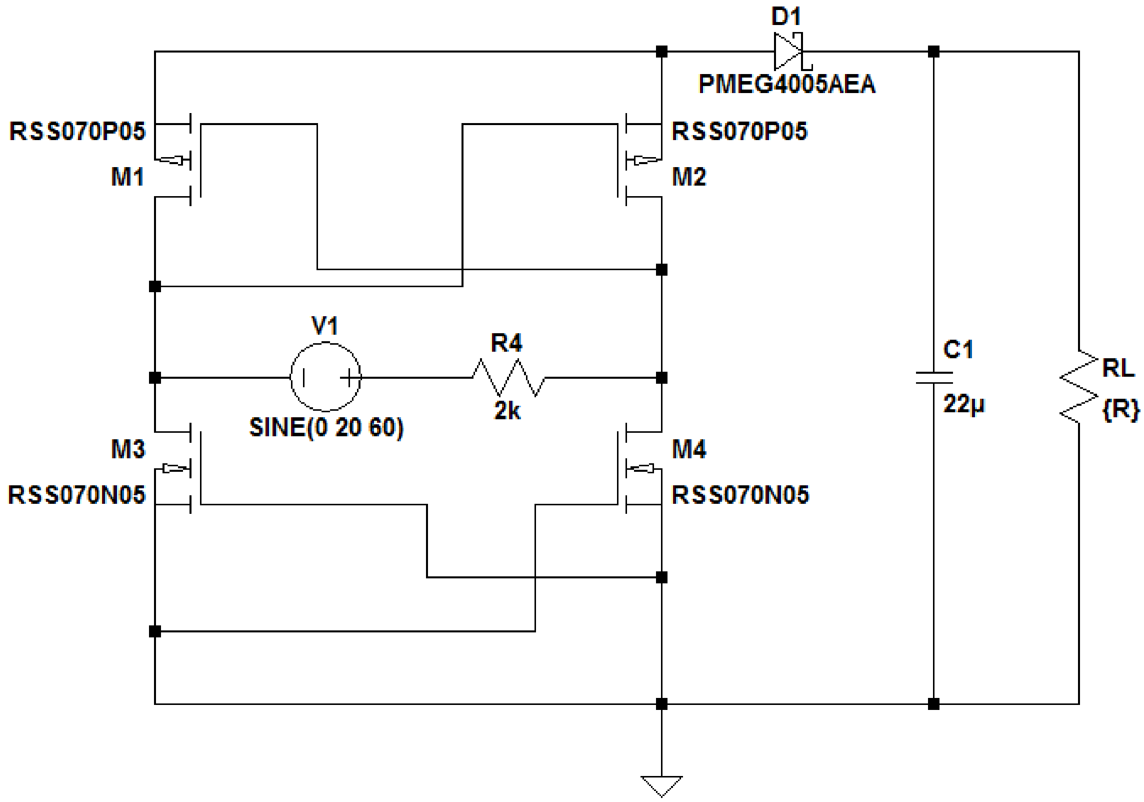

Figure 4.3 LTSpice schematic of negative voltage converter.

In order to find the optimal load resistance for the NVC, a resistance sweep is done. Figure 4.4 shows the waveforms of the resistance sweep. The maximum output power is 20.4 mW, and it occurs at the load resistance of 2 kΩ, and the output voltage is 6.38 V. In Chapter 4.1, the maximum output power of the MFEH is 24.61 mW. So, the efficiency of the NVC can be calculated as follows.

$$\eta_{NVC} = \frac{P_{Out,NVC}}{P_{Max}} \quad (20)$$

And the efficiency of the NVC is 82.9 %.

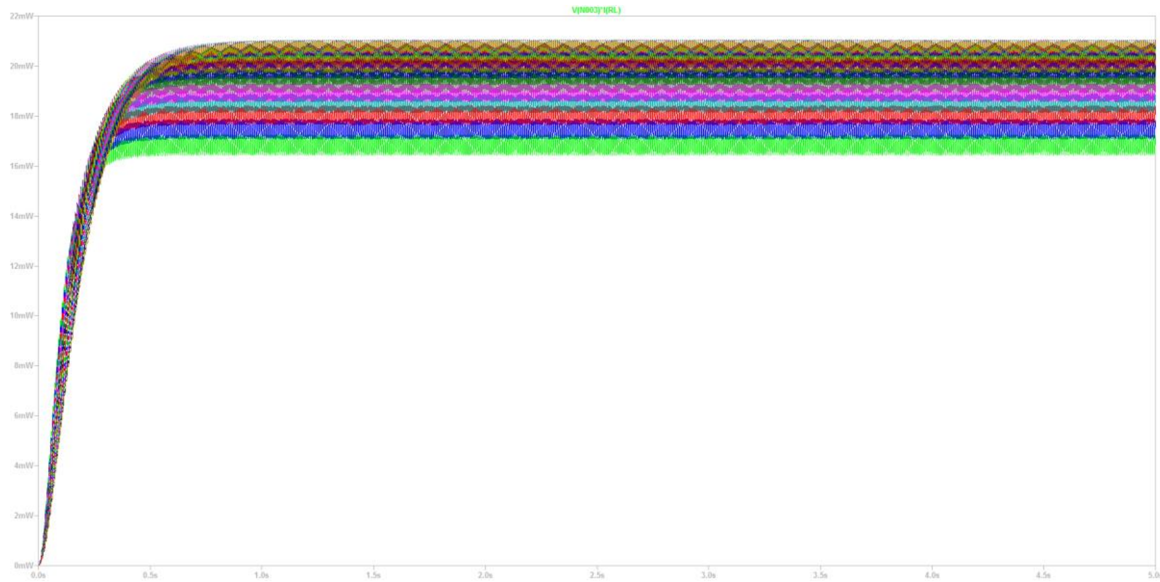

Figure 4.4 Load resistance sweep for NVC.

4.3 Oscillator

Figure 4.5 shows the LTSpice schematic for the oscillator adopted in the proposed circuit. It is a relaxation oscillator built with a comparator. LTC1540 is used in the proposed circuit.

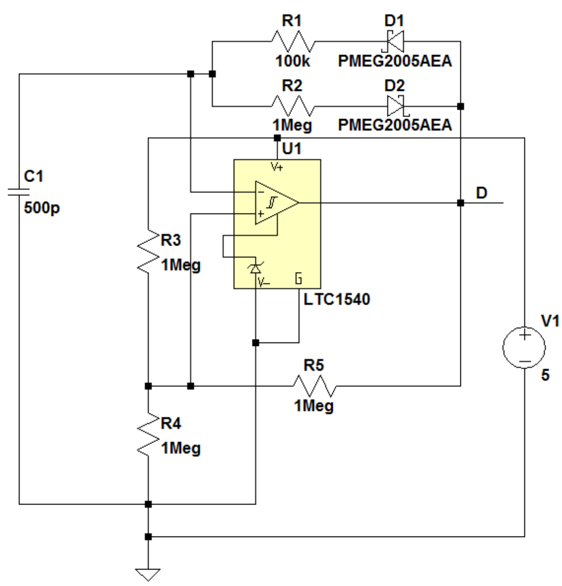

Figure 4.5 LTSpice schematic of oscillator.

By changing the ratio of R_1 and R_2, the duty cycle can be changed. And the operating frequency can be changed by changing the capacitor value of C_1. Note that (17) and (18) are very rough approximation for the duty cycle and frequency of the oscillator. A finer tuning is needed for the oscillator in order to get the desired frequency and duty cycle.

Figure 4.6 shows the simulated waveforms of the oscillator. When R_1 = 100 kΩ, R_2 = 1 MΩ, R_3 = R_4 = R_5 = 1 MΩ, and C_1 = 500 pF, the oscillator generates pulse waves, whose frequency is 3 kHz, and duty cycle is 24.19 %.

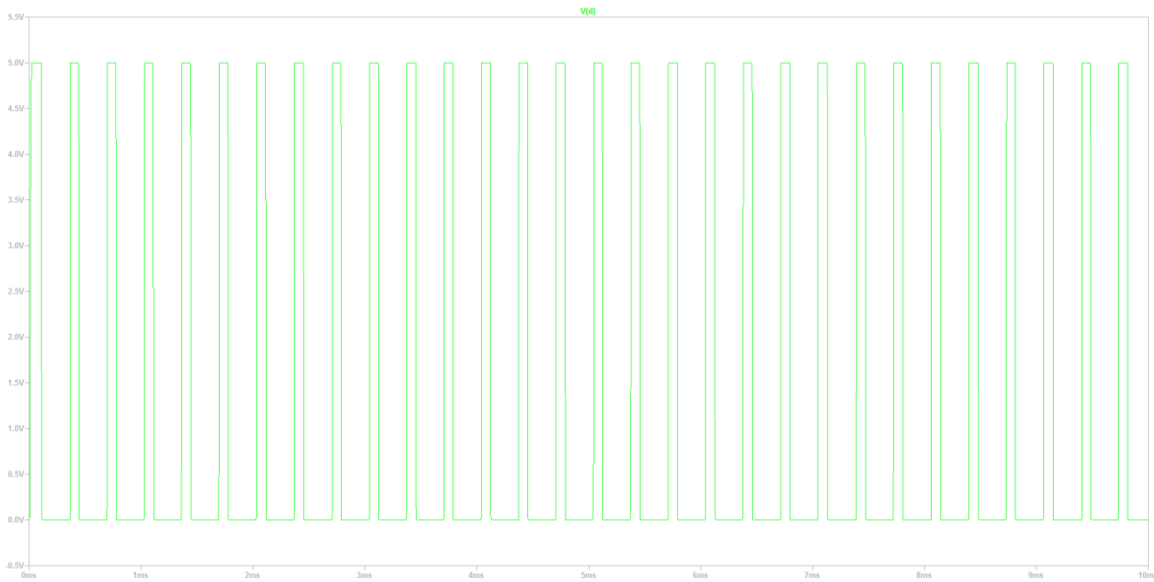

Figure 4.6 Waveforms of oscillator.

4.4 Buck-boost Converter

A buck-boost converter operating in DCM is adopted for impedance matching because of its input resistance characteristics. Figure 4.7 shows the LTSpice schematic of the buck-boost converter integrated with the MFEH modeling circuit as well as NVC. The oscillator is not connected. The inductor is set to 15 mH with an internal resistance of 1 Ω. NMOS RSS070N05 is used for buck-boost converter's switching, and a Schottky diode RB521G-40 is used in the buck-boost converter, with a breakdown voltage of 40 V, and maximum forward current of 0.1 A. The duty cycle and frequency of the buck-boost converter are set to 21% and 3 kHz, respectively.

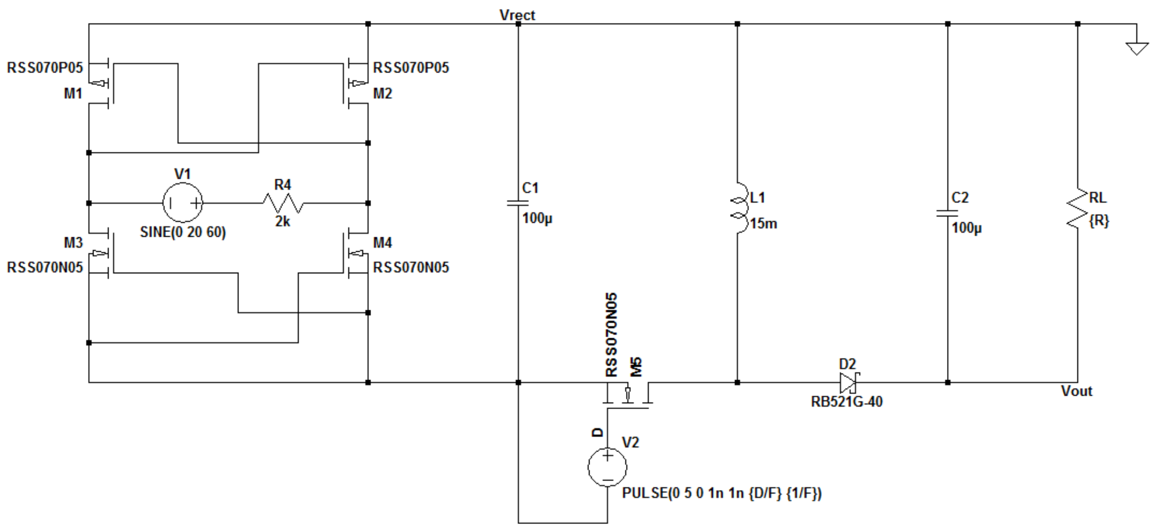

Figure 4.7 LTSpice schematic of the buck-boost converter.

Figure 4.8 shows the output voltage of the NVC, which is 6.54 V. This is very close to the output voltage of the NVC obtained in Chapter 4.2, which is 6.38 V. So, it can be concluded that the source resistance is matched by the load resistance by adopting the buck-boost converter.

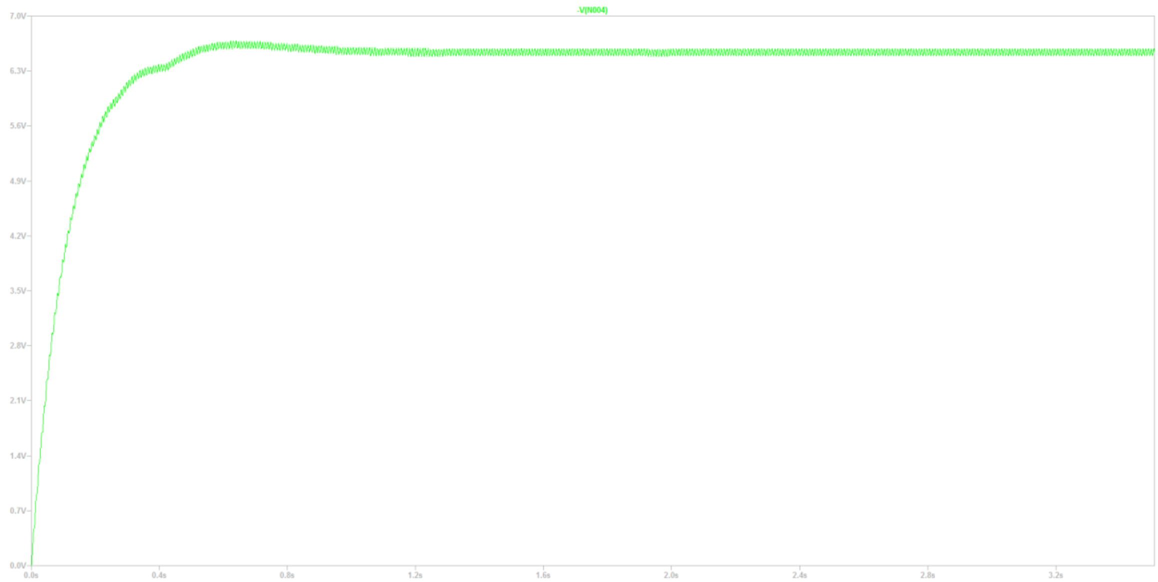

Figure 4.8 Output voltage of the NVC.

In order to find the optimal load resistance for the buck-boost converter, a load resistance sweep is done in LTSpice.

Figure 4.9 plots the output power vs. load resistance of buck-boost converter. In Chapter 2.3.1, we claim that the input resistance of the buck-boost converter is independent of the operating conditions such as input voltage, output voltage and load resistance. However, from Figure 4.9, it can be seen that the input resistance of buck-boost converter is not completely independent of the load resistance. At low load resistance values, the output power is also low, but as the load resistance increases, the output power also increases, and finally stabilizes around 20.09 mW. Although the output power still has a trend of increasing as the load resistance increases, the increment is very small, and it can be concluded that the load resistance matches the source resistance by the buck-boost converter.

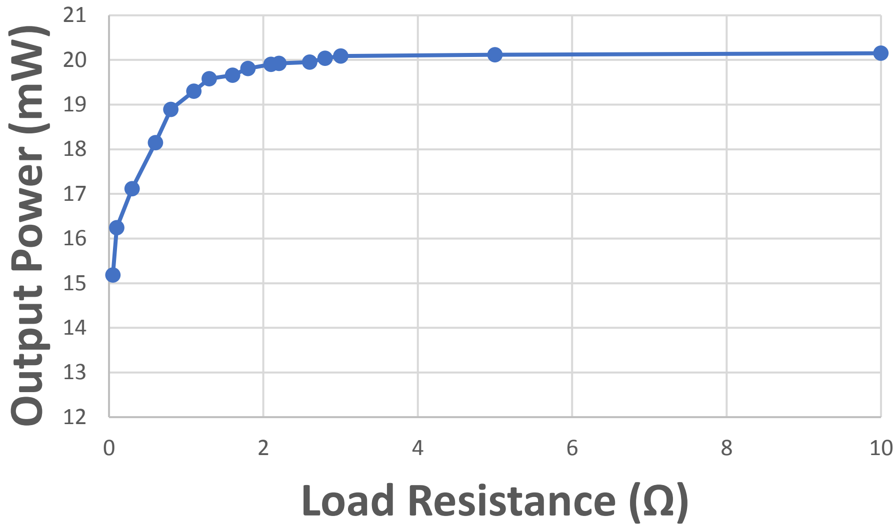

Figure 4.9 Output power vs. load resistance of buck-boost converter.

The efficiency of the buck-boost converter only is calculated as follows. The maximum output power of the NVC is 20.4 mW.

$$\eta_{Buck-boost} = \frac{P_{Out,buck-boost}}{P_{Out,NVC}} \tag{21}$$

And the efficiency of the buck-boost converter is 98.5 %.

To calculate the cumulative efficiency of the buck-boost converter, the reference output power should be the power obtained in Chapter 4.1, which is 24.61 mW. And the efficiency is calculated as follows.

$$\eta_{Buck-boost} = \frac{P_{Out,buck-boost}}{P_{Max}} \tag{22}$$

And the cumulative efficiency of the buck-boost converter is 81.63 %.

4.5 Complete System

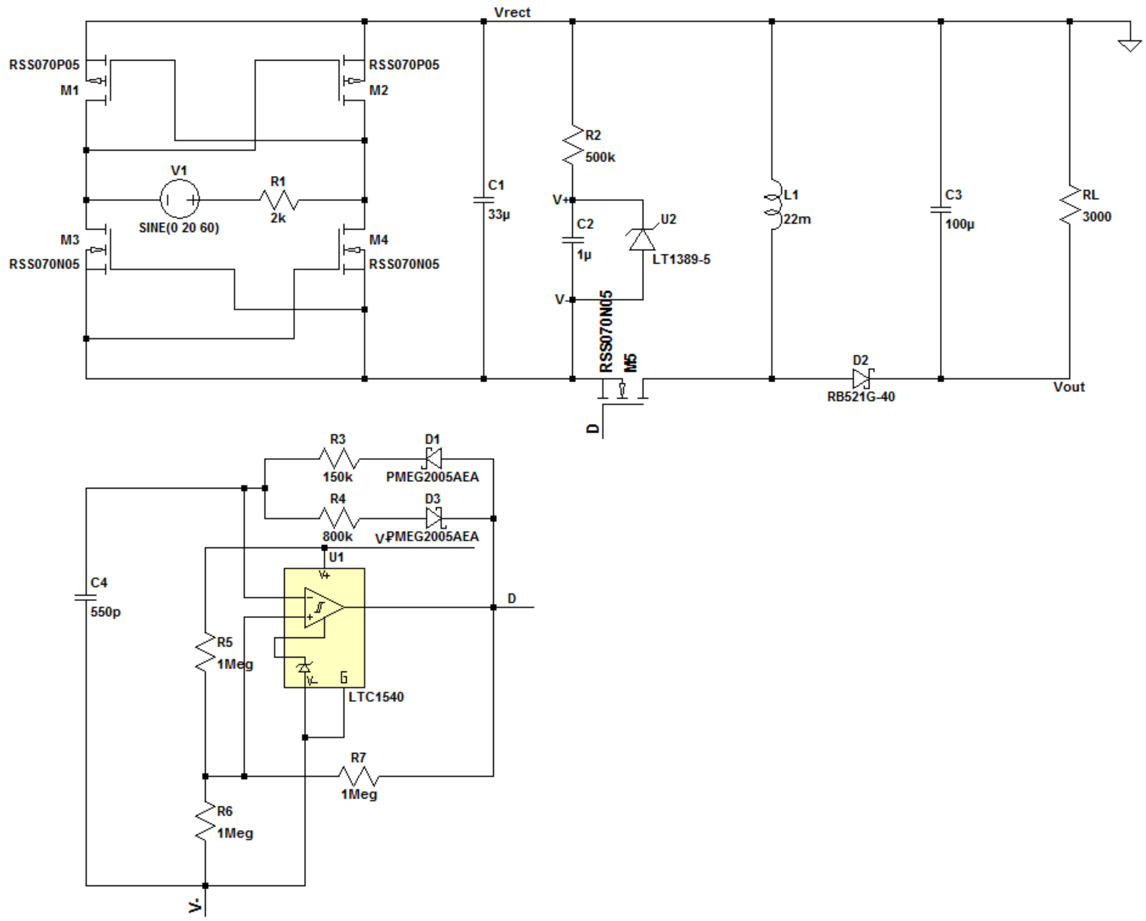

Figure 4.10 LTSpice schematic of the complete system.

Figure 4.10 shows the LTSpice schematic of the complete system. The oscillator is connected to the buck-boost converter. The oscillator is powered by capacitor C_2, which is in series with a resistor R_2. A shunt voltage reference IC LT1389-5 is connected to C_2 in parallel. LT1389-5 works like a Zener diode, and the voltage across C_2 can be limited to 5 V, so that the comparator LTC1540 will not be damaged by overvoltage. Figure 4.11 shows the waveform of the output power of the complete system. The output power of the complete system at the steady state is 20.28 mW.

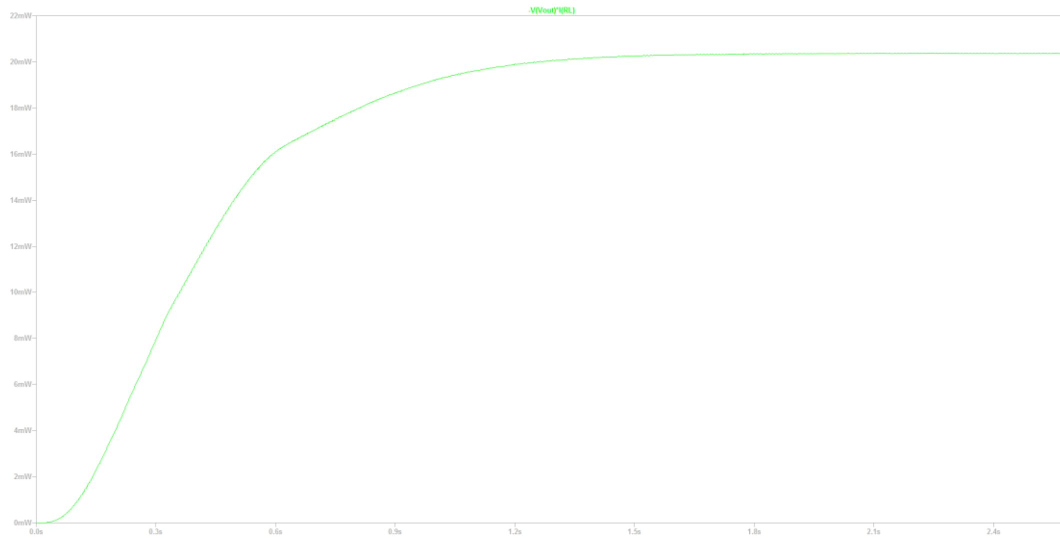

Figure 4.11 Output power of the complete system.

The efficiency of the complete system is calculated as follows, and PMax is 24.61 mW.

$$\eta_{Buck-boost} = \frac{P_{Out,complete\ system}}{P_{Max}} \tag{23}$$

The overall efficiency of the proposed power line energy harvesting system is 82.4 %.

Chapter 5: Measurement Results

In this chapter, the power line energy harvesting system proposed in Chapter 3 is implemented with discrete components on a printed circuit board (PCB). A PCB prototype and experiment setup are shown in section 5.1. The measurement results are presented through section 5.2 – 5.4, which verifies the simulation results in Chapter 4.

5.1 PCB Prototype and Experiment Setup

The MFEH or current transformer is shown in Figure 5.1 and Figure 5.2. The size of the ferrite core is 59 mm by 49 mm. The powerline current of the MFEH ranges from 10 A to 50 A for our experiments.

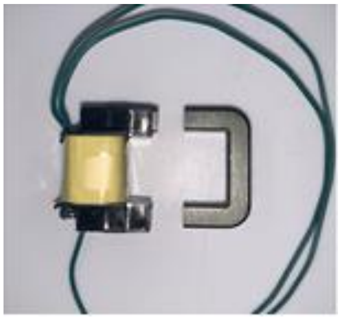

Figure 5.1 Magnetic field energy harvester core.

Figure 5.2 Magnetic field energy harvester with a package.

Figure 5.3 shows a prototype of the proposed PMC and the experiment setup. The size of the PCB is 91 mm by 132 mm.

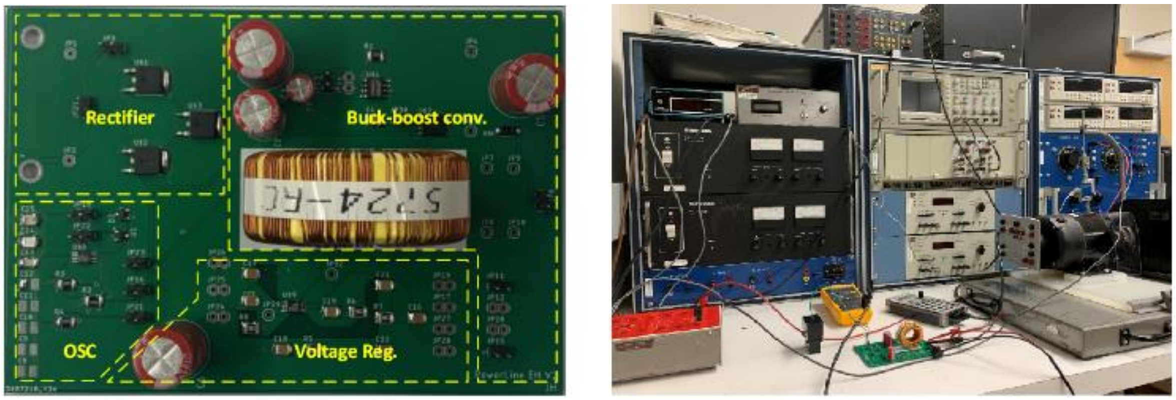

Figure 5.3 Prototype (left) and experiment setup (right).

The proposed PMC with the MFEH is experimented with the powerline current of 10 A, 30 A and 50 A with a frequency of 60 Hz.

To measure the maximum power delivered by the MFEH, we attached a variable resistor at the output of the MFEH, while all other circuit blocks, including the rectifier, the converter and the oscillator, are removed. We measured the maximum power P_{Max} delivered to the resistor with optimal resistance value. To measure the efficiency of the PMC, we attached a variable resistor directly at the output of the buck-boost converter without the voltage regulator and measured the maximum power $P_{Max,buck\text{-}boost}$ with the optimal load resistance value. The efficiency of the proposed PMC is defined as follows.

$$\eta = \frac{P_{Max,buck-boost}}{P_{Max}} \times 100(\%) \tag{24}$$

5.2 Measurement under A Power Line Current of 10 A

Figure 5.4 shows the power P_{Max} delivered to the load resistor by our MFEH with the rectifier under the powerline current of 10 A. The measurement results show that the peak power of 7.96 mW is achieved for the resistance of 2 kΩ, implying the resistance that is required for the input impedance of the buck-boost converter. The power P_{Max} is sensitive to the resistor value, which indicates that impedance matching is necessary for the proposed powerline energy harvesting system.

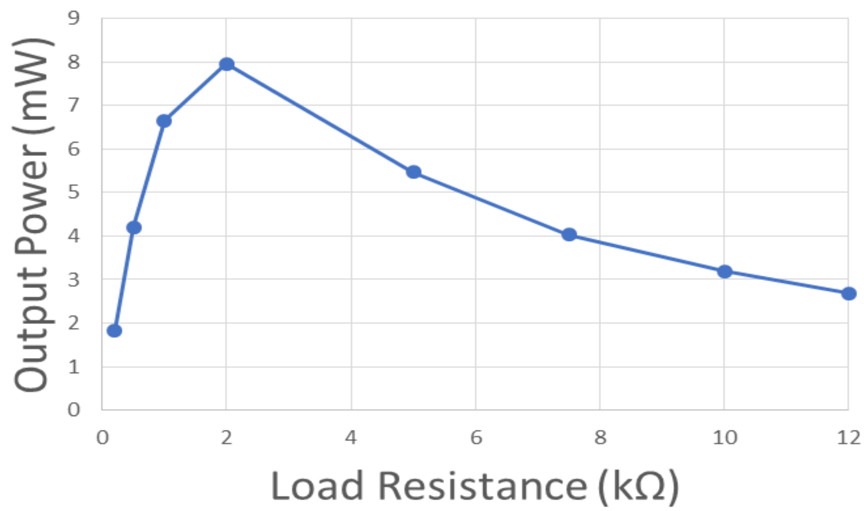

Figure 5.4 Output Power vs. Load Resistance under the powerline current of 10 A.

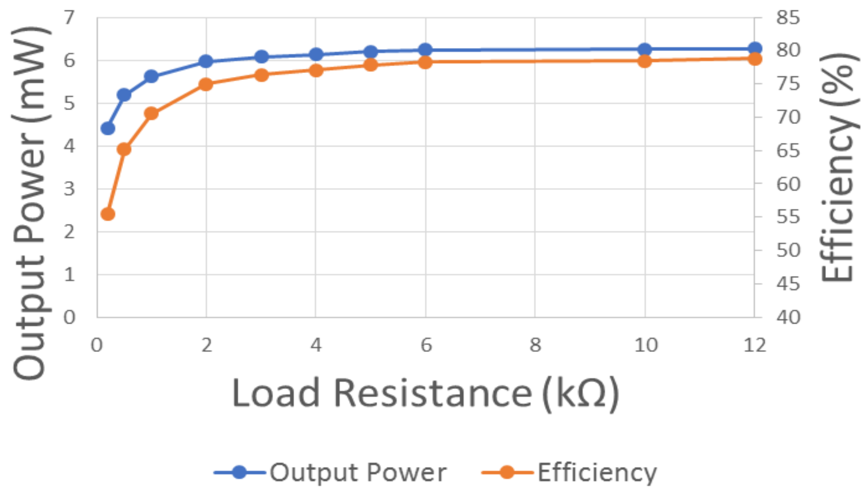

Figure 5.5 Output power and efficiency under the powerline Current of 10 A.

To emulate the optimal resistance of 2 kΩ, the duty cycle D of the buck-boost converter with a 15 mH inductor is set to 21% under the switching frequency of 3 kHz. A variable load resistor is attached in parallel with the capacitor C_O. Figure 5.5 shows the power delivered to the load resistor and its efficiency of the proposed PMC. The output power is somewhat constant for load resistor greater than 2 kΩ. It verifies that the input impedance is the buck-boost converter in DCM is rather insensitive to its load resistor. The peak output power and system efficiency of the system are 6.2 mW and 77.89%, respectively, under the load resistance of 5 kΩ.

5.3 Measurement under A Power Line Current of 30 A

The same measurements are performed for the powerline current of 30 A. Figure 5.6 shows the power delivered to the load resistor by the MFEH. The peak power of 70.21 mW is achieved with the load resistance of 2 kΩ. It implies the source impedance of the MFEH is independent of the powerline current. As the current increases three times, the power would be nine times for an ideal MFEH as a current transformer, but the actual increase is slightly less than that mainly due to the increased loss of the MFEH.

Figure 5.7 plots the output power and system efficiency of the PMC. The peak output power and the peak efficiency are 55.69 mW and 79.32%, respectively, under the load resistance of 5 kΩ. As expected, the efficiency increases as the powerline current increases, but the optimal resistance remains the same.

Figure 5.6 Output Power vs. Load Resistance under the powerline current of 30 A.

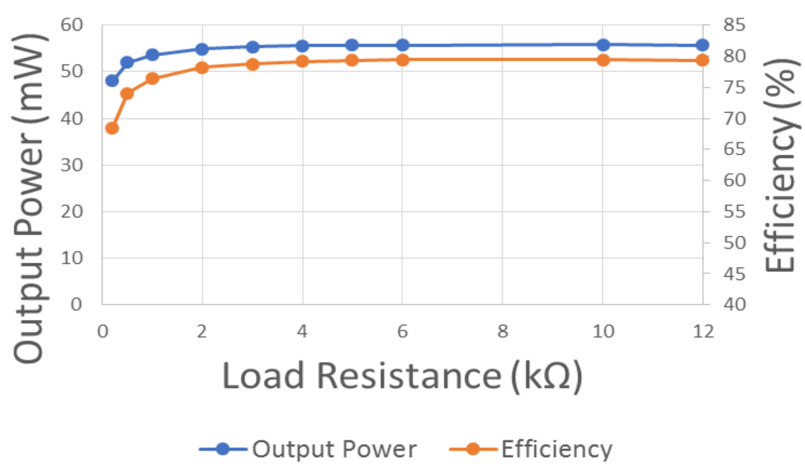

Figure 5.7 Output power and efficiency under the powerline Current of 30 A.

5.4 Measurement under A Power Line Current of 50 A

The measurements are repeated for 50 A. Figure 5.8 shows the peak power of 193.34 mW is achieved for the MFEH at the load resistance of 2 kΩ. Again, it verifies the source impedance of the MFEH is independent of the powerline current. As the current increases five times compared with the case of 10 A, the harvested power increase is 5.66 mW from 199 mW, which is twenty-five times the harvested power with the case of 10 A, implying further increased loss of the MFEH.

Figure 5.9 plots the output power and the efficiency of the PMC. The peak output power and the efficiency of the PMC are 156.6 mW and 80.99%, respectively, under the load resistance of 5 kΩ. The efficiency increases slightly compared with that of 30 A.

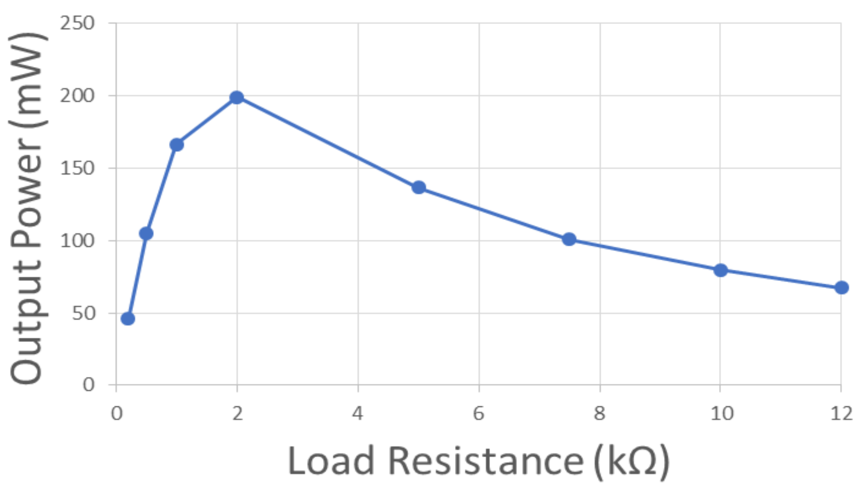

Figure 5.8 Output Power vs. Load Resistance under the powerline current of 50 A.

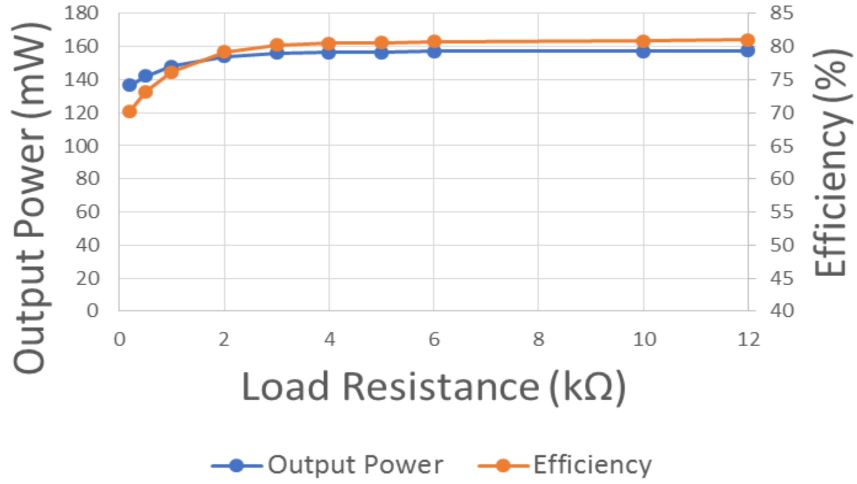

Figure 5.9 Output power and efficiency under the powerline Current of 50 A.

Chapter 6: Conclusion

6.1 Key Contributions

An AC power line energy harvesting circuit is presented in this thesis. The proposed system adopts an MFEH to extract energy from AC powerlines and adopts a buck-boost converter operating in DCM for impedance matching. A wake-up circuit is adopted so that the circuit is capable of cold-start. The proposed PMC is designed to operate for a wide powerline current. The measurement results also indicate that the source impedance of the MFEH remains constant even under a wide range of the powerline current.

6.2 Future Work

In this work, the maximum power point tracking (MPPT) is only analyzed, but not implemented. As the measurement results show, the source impedance of the MFEH is not sensitive to the amplitude, frequency of the input current. So probably in this sense, the impedance matching with MPPT is not necessary. However, as analyzed in Chapter 3, the magnetic core's saturation is a critical issue for power line EH. So, for the future work, the MPPT should be integrated with the core's desaturation, in order to achieve a higher efficiency for the power line energy harvesting system operating under different powerline currents.

References

[1] S. Kim et al., "Ambient RF Energy-Harvesting Technologies for Self-Sustainable Standalone Wireless Sensor Platforms," Proceedings of the IEEE, vol. 102, no. 11, pp. 1649-1666, 2014.

[2] A. Jushi, A. Pegatoquet, and T. N. Le, "Wind Energy Harvesting for Autonomous Wireless Sensor Networks," in 2016 Euromicro Conference on Digital System Design (DSD), 31 Aug.-2 Sept. 2016, 2016, pp. 301-308.

[3] J. H. Hyun, L. Huang, and D. S. Ha, "Vibration and Thermal Energy Harvesting System for Automobiles with Impedance Matching and Wake-up," in 2018 IEEE International Symposium on Circuits and Systems (ISCAS), 27-30 May 2018 2018, pp. 1-5.

[4] Deepti and S. Sharma, "Energy harvesting using piezoelectric for Wireless Sensor Networks," in 2016 IEEE 1st International Conference on Power Electronics, Intelligent Control and Energy Systems (ICPEICES), 4-6 July 2016 2016, pp. 1-3.

[5] Q. Brogan, T. O. Connor, and D. S. Ha, "Solar and thermal energy harvesting with a wearable jacket," in 2014 IEEE International Symposium on Circuits and Systems (ISCAS), 1-5 June 2014 2014, pp. 1412-1415.

[6] P. Kamat, D. Sutar and P. Pavan Prasad, "Efficient Energy Harvesting Using Current Tranformer for Smart Grid Application," 2018 2nd International Conference on Trends in Electronics and Informatics (ICOEI), Tirunelveli, 2018, pp. 343-347.

[7] X. Zhao, T. Keutel, M. Baldauf and O. Kanoun, "Energy harvesting for overhead power line monitoring," International Multi-Conference on Systems, Signals & Devices, Chemnitz, 2012, pp. 1-5.

[8] Y. Zhuang, C. Xu, S. Yuan, C. He, A. Chen, W. W. Lee, J. Zhou, and Y. Huang, "An improved energy harvesting system on power transmission lines," in 2017 IEEE Wireless Power Transfer Conference (WPTC), 2017.

[9] K. Tashiro, H. Wakiwaka, S. Inoue, and Y. Uchiyama, "Energy Harvesting of Magnetic Power-Line Noise," IEEE Transactions on Magnetics, vol. 47, no. 10, pp. 4441-4444, 2011.

[10] T. Taithongchai and E. Leelarasmee, "Adaptive electromagnetic energy harvesting circuit for wireless sensor application," in 2009 6th International Conference on Electrical Engineering/Electronics, Computer, Telecommunications and Information Technology, 6-9 May 2009 2009, vol. 01, pp. 278-281.

[11] J. D. Boles, B. Ozpineci, L. M. Tolbert, T. A. Burress, C. W. Ayers, and J. A. Baxter, "Inductive power harvesting for a touchless transmission line inspection system," in 2016 IEEE Power and Energy Society General Meeting (PESGM), 17-21 July 2016 2016, pp. 1-5.

[12] A. Abasian, A. Tabesh, A. Z. Nezhad, and N. Rezaei-Hosseinabadi, "Design Optimization of an Energy Harvesting Platform for Self-Powered Wireless Devices in Monitoring of AC Power Lines," IEEE Transactions on Power Electronics, vol. 33, no. 12, pp. 10308-10316, 2018.

[13] T. Hosseinimehr and A. Tabesh, "Magnetic Field Energy Harvesting from AC Lines for Powering Wireless Sensor Nodes in Smart Grids," in IEEE Transactions on Industrial Electronics, vol. 63, no. 8, pp. 4947-4954, Aug. 2016.

[14] S. Yuan, Y. Huang, J. Zhou, Q. Xu, C. Song and P. Thompson, "Magnetic Field Energy Harvesting Under Overhead Power Lines," in IEEE Transactions on Power Electronics, vol. 30, no. 11, pp. 6191-6202, Nov. 2015.

[15] K. Tashiro, H. Wakiwaka, S. Inoue and Y. Uchiyama, "Energy Harvesting of Magnetic Power-Line Noise," in IEEE Transactions on Magnetics, vol. 47, no. 10, pp. 4441-4444, Oct. 2011.

[16] F. Guo, H. Hayat and J. Wang, "Energy harvesting devices for high voltage transmission line monitoring," 2011 IEEE Power and Energy Society General Meeting, Detroit, MI, USA, 2011, pp. 1-8.

[17] H. Tzu-Chi, Y. Yao-Yi, L. Yu-Huei, D. Ming-Jhe, C. Shih-Hsien, and C. Ke-Horng, "A battery-free energy harvesting system with the switch capacitor sampler (SCS) technique for high power factor in smart meter applications," in 2011 IEEE/IFIP 19th International Conference on VLSI and System-on-Chip, 3-5 Oct. 2011 2011, pp. 359-362.

[18] S. Yuan, Y. Huang, J. Zhou, Q. Xu, C. Song, and G. Yuan, "A High-Efficiency Helical Core for Magnetic Field Energy Harvesting," IEEE Transactions on Power Electronics, vol. 32, no. 7, pp. 5365-5376, 2017.

[19] G. Yu, Z. Donglai, and H. Zhu, "Adaptive impedance matching optimal control method for cascaded DC-DC power supply system," in IECON 2017 - 43rd Annual Conference of the IEEE Industrial Electronics Society, 29 Oct.-1 Nov. 2017 2017, pp. 751-755.

[20] Y. Xu, D. S. Ha, and M. Xu, "Energy harvesting circuit with input matching in boundary conduction mode for electromagnetic generators," in 2017 IEEE International Symposium on Circuits and Systems (ISCAS), 28-31 May 2017 2017, pp. 1-4.

[21] Y. Huang, N. Shinohara, and T. Mitani, "Theoretical analysis on DC-DC converter for impedance matching of a rectifying circuit in wireless power transfer," in 2015 IEEE International Symposium on Radio-Frequency Integration Technology (RFIT), 26-28 Aug. 2015, 2015, pp. 229-231.

[22] N. Kong, D. S. Ha, A. Erturk, and D. J. Inman, “Resistive impedance matching circuit for piezoelectric energy harvesting,” Journal of Intelligent Material Systems and Structures, vol. 21, no. 13, pp. 1293–1302, September 2010.

[23] J. P. M. Figueiredo, F. L. Tofoli and R. L. Alves, "Comparison of nonisolated dc-dc converters from the efficiency point of view," XI Brazilian Power Electronics Conference, Praiamar, 2011, pp. 14-19.

[24] Y. Jiang, J. A. A. Qahouq, and T. A. Haskew, "Adaptive Step Size With Adaptive-Perturbation-Frequency Digital MPPT Controller for a Single-Sensor Photovoltaic Solar System," IEEE Transactions on Power Electronics, vol. 28, no. 7, pp. 3195-3205, 2013.

[25] S. Gaikwad and M. Ghosal, "Energy efficient storage-less and converter-less renewable energy harvesting system using MPPT," 2017 2nd International Conference for Convergence in Technology (I2CT), Mumbai, 2017, pp. 971-973.

[26] Q. Sun, S. Patil, N. Sun, and B. Lehman, "Modeling and optimization of an inductive magnetic harvester considering nonlinear effects," in 2013 IEEE 14th Workshop on Control and Modeling for Power Electronics (COMPEL), 23-26 June 2013, 2013, pp. 1-6.

[27] Y. Zhuang et al., "Improving Current Transformer-Based Energy Extraction from AC Power Lines by Manipulating Magnetic Field," in IEEE Transactions on Industrial Electronics, vol. 67, no. 11, pp. 9471-9479, Nov. 2020.

[28] I. M. Darmayuda et al., "A Self-Powered Power Conditioning IC for Piezoelectric Energy Harvesting From Short-Duration Vibrations," in IEEE Transactions on Circuits and Systems II: Express Briefs, vol. 59, no. 9, pp. 578-582, Sept. 2012.

[29] Y. Gao, D. I. Made, S. J. Cheng, M. Je and C. H. Heng, "An energyautonomous piezoelectric energy harvester interface circuit with 0.3V startup voltage," 2013 IEEE Asian Solid-State Circuits Conference (ASSCC), Singapore, pp. 445-448, 2013.

[30] D. Niu, Z. Huang, M. Jiang and Y. Inoue, "A sub-0.3V CMOS rectifier for energy harvesting applications," 2011 IEEE 54th International Midwest Symposium on Circuits and Systems (MWSCAS), Seoul, pp. 1-4, 2011.

[31] Y. Huang, N. Shinohara and T. Mitani, "Impedance Matching in Wireless Power Transfer," in IEEE Transactions on Microwave Theory and Techniques, vol. 65, no. 2, pp. 582-590, Feb. 2017.

[32] X. Zeng, B. Li, H. Li, S. Chen, and Y. Chen, "Non-invasive energy harvesting for wireless sensors from electromagnetic fields around 10kV three-core power cables," in 2017 1st International Conference on Electrical Materials and Power Equipment (ICEMPE), 14-17 May 2017, 2017, pp. 536-539.